scientific reports

Check for updates

OPEN

Experimental quantum state discrimination using the optimal fixed rate of inconclusive outcomes strategy

Santiago Gómez[1,2], Esteban S. Gómez[1,2]✉, Omar Jiménez[3], Aldo Delgado[1,2], Stephen P. Walborn[1,2] & Gustavo Lima[1,2]

The problem of non-orthogonal state discrimination underlies crucial quantum information tasks, such as cryptography and computing protocols. Therefore, it is decisive to find optimal scenarios for discrimination among quantum states. We experimentally investigate the strategy for the optimal discrimination of two non-orthogonal states considering a fixed rate of inconclusive outcomes (FRIO). The main advantage of the FRIO strategy is to interpolate between unambiguous and minimum error discrimination by solely adjusting the rate of inconclusive outcomes. We present a versatile experimental scheme that performs the optimal FRIO measurement for any pair of generated non-orthogonal states with arbitrary a priori probabilities and any fixed rate of inconclusive outcomes. Considering different values of the free parameters in the FRIO protocol, we implement it upon qubit states encoded in the polarization mode of single photons generated in the spontaneous parametric down-conversion process. Moreover, we resort to a newfangled double-path Sagnac interferometer to perform a three-outcome non-projective measurement required for the discrimination task, showing excellent agreement with the theoretical prediction. This experiment provides a practical toolbox for a wide range of quantum state discrimination strategies using the FRIO scheme, which can significantly benefit quantum information applications and fundamental studies in quantum theory.

Quantum measurements lie at the core of quantum mechanics and are a cornerstone of interpretations of quantum theory[1]. Moreover, they have a crucial role in the evolution of quantum systems[2] and have found appealing applications such as estimating unknown physical parameters using quantum resources[3,4]. In quantum information science, measurements are especially relevant for implementing quantum computing and communication protocols[5]. The simplest scenario involves two parties, where a sender can prepare and send information encoded in quantum states[6]. To access to this information, the receiver has to choose which quantum measurement will be performed[7,8]. Usually, the chosen measurement will depend on the properties of the received states and the features of the quantum protocol to be implemented. One possible task is identifying an unknown quantum state. One way to address this situation lies in the quantum tomography technique, which reconstructs the quantum state of an unknown physical system from the measured probabilities of a suitable set of observables. Nevertheless, the number of measurements required for a successful state reconstruction scales at least polynomially in the dimension of the state[9], and requires multiple identical copies. Other tasks require identifying quantum states among others belonging to a given set in a single-shot measurement. However, performing this assignment is impossible deterministically when non-orthogonal states are considered.

Hence, quantum state discrimination (QSD) relies on identifying a quantum state belonging to a set of N known non-orthogonal quantum states. This task plays a fundamental role in several remarkable quantum protocols such as quantum key distribution[10], quantum teleportation[11,12], entanglement swapping[13,14], and entanglement concentration[15,16]. Moreover, being a fundamental protocol, QSD also has been studied in relation with: contextuality[17], path distinguishability[18–20], and quantum correlations[21–23]. Thus, there are well-known strategies to implement QSD, namely the *minimum error discrimination* (MED)[24,25], the *unambiguous discrimination*

[1]Departamento de Física, Universidad de Concepción, Casilla 160-C, Concepción, Chile. [2]Millennium Institute for Research in Optics, Universidad de Concepción, Casilla 160-C, Concepción, Chile. [3]Centro de Óptica e Información Cuántica, Facultad de Ciencias, Universidad Mayor, Camino La Pirámide No 5750, Huechuraba, Santiago, Chile. ✉email: estesepulveda@udec.cl

(UD)[26–29], and the *maximum confidence discrimination* (MCD)[30–32], each focused on optimizing some figure of merit[33]. To implement any QSD strategy, it is necessary first to determine the corresponding measurement defined by a set of positive operator-valued measures (POVMs)[34,35], and then engineer a way to implement these POVMs in an experimental realization[36,37]. In the case of MED, there are N POVM elements Π_i associated with the discrimination of one of the states ρ_i[7]. However, since the given states are non-orthogonal, the discrimination process will inevitably introduce errors in identifying each quantum state ρ_i[24]. In the MED strategy, the average error probability is minimized[25,38]. Conversely, UD has no error in identifying each quantum state ρ_i. This process can be achieved by introducing an additional POVM element, Π_0, which is associated with an inconclusive outcome[28]. Finally, the MCD strategy maximizes the confidence in taking the measurement outcome i to indicate that the ρ_i state was prepared[8]. QSD has been experimentally implemented for MED[39–44], UD[45–48] and also for MCD[49,50]. Moreover, the experimental realization for maximizing the mutual information[51] between two users was also performed[52].

The discrimination of unknown quantum states also has been studied. In this case, the communicating parties have no information about the states to be discriminated. Remarkably, it has been demonstrated that discrimination is feasible even in this situation. This is achieved through a programmable discriminator[53–58], that is, a device where the unknown states to be discriminated are stored. In particular, it has been shown that this programmable discriminator is universal and attains a success probability close to the optimum of unambiguous state discrimination. In addition, the discrimination between two known families of non-orthogonal quantum states has been studied from the point of view of neural networks[59,60]. Nevertheless, implementing it is highly costly since the device requires a priori stored information and additional ancilla systems to work properly.

Under certain conditions, the MED and UD strategies coincide with the MCD strategy[31,61]. Moreover, MED and UD can be joined simultaneously in a more general QSD scheme known as fixed rate of inconclusive outcomes (FRIO)[62–64]. In the case of QSD by FRIO, the average error probability in identifying the quantum state ρ_i is minimized under the condition of fixing the probability of inconclusive results[65]. Although for MED, UD and MCD there is no analytical solution to the discrimination by FRIO of N arbitrary non-orthogonal states[66], in the case of two pure non-orthogonal states with arbitrary a *priori* preparation probabilities, the complete optimal solution is known[61,67]. Moreover, experimental schemes for the realization of FRIO onto two pure non-orthogonal states have been proposed[68,69].

Here we present an experimental realization of FRIO discrimination on two pure non-orthogonal states encoded on the polarization state of single photons created by the spontaneous parametric down-conversion (SPDC) process. We use a double-path Sagnac interferometer to implement a genuine three-outcome POVM over a single polarization qubit performing the required measurement. A notable feature of our experimental setup is that it can be easily configured to implement the optimal FRIO POVM for all pairs of non-orthogonal states, arbitrary a priori probabilities, and any value of the fixed rate of the inconclusive outcome. In particular, it allows us to implement MED, UD, and any intermediate case of FRIO by fixing the rate of inconclusive outcomes, showing a good agreement with the theoretical results[61,67]. This experimental platform gives a flexible and customizable toolbox for a wide range of QSD strategies involving the FRIO scheme, which can be helpful in exploring novel applications for quantum information protocols and further research in quantum foundations.

Methods

We consider a qubit source of two pure non-orthogonal states denoted by $|\phi_1\rangle$ and $|\phi_2\rangle$, with *a priori* preparation probabilities η_1 and η_2, respectively. Without loss of generality, these states can be written as

$$|\phi_1\rangle = \cos\alpha|0\rangle + \sin\alpha|1\rangle,$$
$$|\phi_2\rangle = \cos\alpha|0\rangle - \sin\alpha|1\rangle,$$

where the states $\{|0\rangle, |1\rangle\}$ represent the logical basis. The overlap between the states is given by the parameter $s = \langle\phi_1|\phi_2\rangle = \cos(2\alpha)$, considering $s \in [0, 1]$. Moreover, the *a priori* probabilities can be set arbitrarily and they must satisfy the constraint $\eta_1 + \eta_2 = 1$. The FRIO discrimination process is carried out by using three POVM elements, where $\Pi_{1(2)}$ is associated to the identification of $|\phi_{1(2)}\rangle$ and Π_0 corresponds to the inconclusive outcome, where no information of the states can be learned from the measurement. These three operators satisfy the condition

$$\Pi_1 + \Pi_2 + \Pi_0 = \mathbb{1},$$

where $\mathbb{1}$ is the identity operator. We define the following probabilities $p_{1(2)}$, $r_{1(2)}$ and $q_{1(2)}$, corresponding to the probabilities of success, error and the inconclusive outcome, respectively, in the discrimination of $|\phi_{1(2)}\rangle$. These probabilities encompass all possible outcomes in this case, that is $p_{1(2)} + r_{1(2)} + q_{1(2)} = 1$.

The average probabilities of success P_s, error P_e and inconclusive outcome Q over the states, are given by[61]

$$\begin{aligned} P_s &= tr(\eta_1\rho_1\Pi_1) + tr(\eta_2\rho_2\Pi_2) = \eta_1 p_1 + \eta_2 p_2, \\ P_e &= tr(\eta_1\rho_1\Pi_2) + tr(\eta_2\rho_2\Pi_1) = \eta_1 r_1 + \eta_2 r_2, \\ Q &= tr(\rho\Pi_0) = \eta_1 q_1 + \eta_2 q_2, \end{aligned} \tag{1}$$

where $\rho_{1(2)} = |\phi_{1(2)}\rangle\langle\phi_{1(2)}|$, and $\rho = \eta_1\rho_1 + \eta_2\rho_2$. It is straightforward to see that the average probabilities satisfy $P_s + P_e + Q = 1$.

Optimal strategy for FRIO discrimination. The optimal FRIO strategy minimizes the average error probability P_e under the constraint that the inconclusive outcome probability Q is fixed. For this case, the opti-

mal probabilities for FRIO were obtained by Bagan et al.[61]. Due to the symmetry of this task, it is enough to consider the case $\eta_1 \leq \eta_2$, that is, when $0 \leq \eta_1 \leq 1/2$. The FRIO solution identifies three intervals where the optimal probabilities can be obtained. These intervals depend on the overlap values s and the probability η_1 given a fixed value of Q[61,67]. Interval I is defined as

$$\frac{s^2}{1+s^2} \leq \eta_1 \leq 1/2 \quad \text{and} \quad 0 \leq Q \leq Q_0,$$

where $Q_0 = 2s\sqrt{\eta_1\eta_2}$ is the maximum inconclusive event probability for this interval. Interval II is defined as

$$0 \leq \eta_1 \leq \frac{s^2}{1+s^2} \text{and} 0 \leq Q \leq Q_{th},$$

with $Q_{th} = \frac{2\eta_1\eta_2(1-s^2)}{1-Q_0}$ a threshold value that separates intervals II and III. The optimal probabilities for these intervals are given by

$$\begin{aligned} q_i &= \frac{Q}{2\eta_i}, \\ r_i &= \frac{1}{2}\left(1 - q_i - \frac{(1-q_i)\overline{Q} - \frac{(Q_0-Q)^2}{2\eta_i}}{\sqrt{\overline{Q}^2 - (Q_0-Q)^2}}\right), \\ p_i &= 1 - q_i - r_i, \end{aligned}$$

for $i = 1, 2$, and $\overline{Q} = 1 - Q$. Therefore, the optimal error probability P_e valid in intervals I and II is minimal and reads

$$P_e = \frac{1}{2}\left(\overline{Q} - \sqrt{\overline{Q}^2 - (Q_0 - Q)^2}\right).$$

On the other hand, the interval III is defined when

$$0 \leq \eta_1 \leq \frac{s^2}{1+s^2} \quad \text{and} \quad Q_{\text{th}} \leq Q \leq \eta_1 + \eta_2 s^2,$$

and the optimal probabilities are given by

$$\begin{aligned} p_1 &= 0, r_1 = \frac{P_e}{\eta_1}, q_1 = 1 - r_1, r_2 = 0, \\ p_2 &= \left(s\sqrt{r_1} + \sqrt{(1-r_1)(1-s^2)}\right)^2, q_2 = 1 - p_2, \end{aligned}$$

and the optimal average error probability is given by[67]

$$P_e = \frac{1}{1-4c}\left(\eta_1\overline{Q} + c(\eta_2 - \eta_1 - 2\overline{Q}) - Q_0\sqrt{c(Q\overline{Q} - c)}\right),$$

where $c = \eta_1\eta_2(1-s^2)$. Note that the optimal strategy in interval III is implemented using a two-outcome projective measurement.

A notable feature of FRIO discrimination is that allows not only MED (when $Q = 0$) and UD (when $Q = Q_{max}$), but also intermediate cases. Here, Q_{max} is the maximum possible value for Q in each interval defined above. To show the versatility of this state discrimination scheme, we present an optical experiment performing FRIO for both cases (MED and UD), and we consider an intermediate case for the inconclusive event $Q = Q_0/2$ using the same device implementing the required POVMs in Eq. (1) for each interval. The optimal POVM implementation depends on the overlap s between the non-orthogonal qubit states $\{|\phi_i\rangle\}$. These states are prepared by encoding the polarization modes (horizontal and vertical directions) of single photons generated using a heralded source based on the SPDC process. We are able to finely tuning the parameter s and the a *priori* preparation probabilities η_i, performing FRIO strategies ($Q = 0, Q = Q_0/2$, and $Q = Q_{max}$) considering seven values of the overlap s in two preparation scenarios, when $\eta_1 = \eta_2$ and $\eta_1 < \eta_2$.

Experimental description. To carry out FRIO quantum state discrimination, we implement a heralded photon source based on the spontaneous parametric down-conversion (SPDC) process and a two-path Sagnac interferometer to perform the required measurement. The experimental setup is depicted in Fig. 1. A continuous-wave laser at 405 nm pumps a type-II nonlinear periodically poled potassium titanyl phosphate (PPKTP) crystal to create degenerate down-converted photons at 810 nm with horizontal and vertical polarization. To ensure the degenerate phase-matching conditions and remove the remaining pump beam, a Semrock high-quality narrow bandpass filter centered at 810 nm is used, with 0.5 nm of bandwidth and a peak transmission of $> 90\%$. To maximize the coincidence count rate, we consider a numerical model[70]. Precisely, the optimal coupling condition is reached when $\omega_{DCP} = \sqrt{2}\omega_p$, where ω_p and ω_{DCP} are the waist modes of the pump beam and the down-converted photons at the center of the PPKTP crystal, respectively. In our case, these waists are adjusted using a 20 cm focal length lens L and $10\times$ objective lenses.

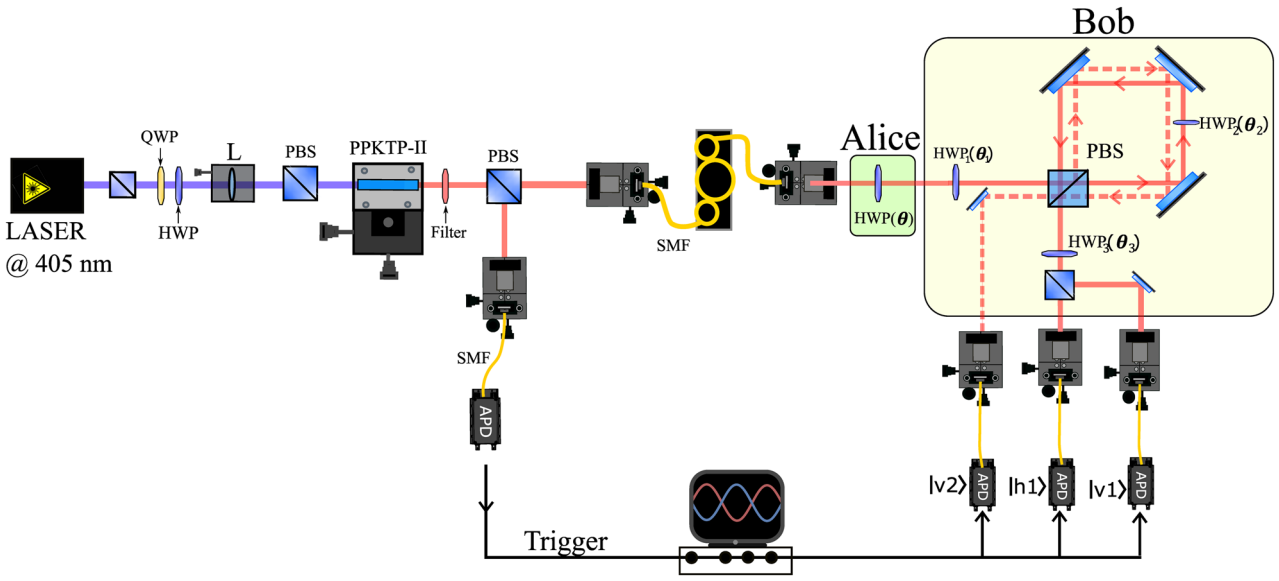

Figure 1. Experimental setup used to implement FRIO quantum state discrimination. Alice can prepare the non-orthogonal state $|\phi_i\rangle$ using the half-wave plate $HWP(\theta)$, encoding on a single photon generated at the heralded source based on the SPDC process. Bob uses a two-path Sagnac interferometer to perform the three-outcomes POVM needed for the chosen discrimination strategy covered by the FRIO scheme. Each outcome is associated with success, error, and inconclusive results. In particular, for intervals I and II, the inconclusive outcome Q is detected in the spatial mode labeled by $|V2\rangle$. Thus, the state $|\phi_1\rangle$ is identified when $|V1\rangle$ is detected, while the $|\phi_2\rangle$ is associated to detecting in $|H1\rangle$. See the main text for more details.

The generated photon pairs can be used to implement a heralded single-photon source, in the sense that one down-converted photon arrives at the trigger detector announcing the passage of the other photon through the stages of Alice and Bob (see Fig. 1). Therefore, a polarizing beam splitter (PBS) is placed after the PPKTP crystal to separate the down-converted photons deterministically. Then, they are sent to the trigger and Alice section coupling into single-mode optical fibers (SMF), removing any spatial correlation between them that could arise from imperfections when satisfying the phase-matching conditions in the crystal. Moreover, to maintain the polarization state of the photons through the propagation in the optical fiber, we use a manual fiber polarization controller for the photon arriving at Alice, and polarizing films are placed in front of the trigger and Alice's detectors to ensure the correct polarization mode of the detected state.

Alice can prepare the two non-orthogonal states $\{|\phi_1\rangle, |\phi_2\rangle\}$ using the half-wave plate HWP(θ) to encode a polarization qubit her photon. The polarization qubit states read

$$\begin{aligned} |\phi_1\rangle &= \cos 2\theta |H\rangle + \sin 2\theta |V\rangle, \\ |\phi_2\rangle &= \cos 2\theta |H\rangle - \sin 2\theta |V\rangle, \end{aligned} \tag{2}$$

where $|H\rangle$ and $|V\rangle$ are the horizontal and vertical polarization modes, and θ is the inclination angle of the HWP with respect to its fast axis. The photons are sent to Bob through free space to implement the FRIO state discrimination procedure. To generate the global unitary transformation U over the non-orthogonal states required to implement the POVM[69], we resort to couple the polarization degree of freedom with two spatial propagation modes as an ancilla system. First, Bob rotates the polarization state using a half-wave plate HWP_1 oriented at angle θ_1 and then inputs the state to the two-path Sagnac interferometer configuration, which is composed of three laser mirrors, the HWP_2 and a PBS. In this device the polarization is coherently coupled with the spatial modes[71–73], since the PBS splits the incident photon through the clockwise (reflected) or counterclockwise (transmitted) mode inside the interferometer. Thus, the PBS operation can be seen as a controlled-NOT gate: the photon populates a spatial mode depending on the input polarization state. Moreover, in the counterclockwise path, HWP_2 is aligned at angle θ_2, which rotates the photon's polarization again if it propagates in this spatial mode. Then, a new passage through the same PBS superposes the two spatial modes. We denote the initial and second photon propagation paths by $|1\rangle$ and $|2\rangle$. Lastly, an HWP_3 at θ_3 and a PBS are placed in the $|1\rangle$ mode to obtain three outcomes that determine the required POVM. The global unitary can be written as

$$U = C(\theta_3) \cdot CNOT \cdot C(\theta_2) \cdot CNOT \cdot C(\theta_1),$$

where the transformation $C(\theta_i)$ represents a rotation of the polarization in an angle $2\theta_i$. Then, applying U onto the non-orthogonal states $\{|\phi_1\rangle, |\phi_2\rangle\}$ gives us the following transformation,

$$\begin{aligned} U|\phi_1\rangle|1\rangle &= \sqrt{p_1}|V\rangle|1\rangle + \sqrt{r_1}|H\rangle|1\rangle + \sqrt{q_1}|V\rangle|2\rangle, \\ U|\phi_2\rangle|1\rangle &= \sqrt{r_2}|V\rangle|1\rangle + \sqrt{p_2}|H\rangle|1\rangle + \sqrt{q_2}|V\rangle|2\rangle, \end{aligned} \tag{3}$$

where the parameters p_i, r_i, and q_i are the optimal success, error, and inconclusive outcome probabilities associated to discriminate $|\phi_i\rangle$. Indeed, for the case when $\eta_1 = \eta_2 = 1/2$ (that is, equal state preparation), we can write these optimal probabilities in terms of the waveplate angles θ and $\theta_1, \theta_2, \theta_3$:

$$\begin{aligned} p_i &= \frac{1}{2}(\cos 2\theta \cos\theta_2 + \sin 2\theta)^2, \\ r_i &= \frac{1}{2}(\cos 2\theta \cos\theta_2 - \sin 2\theta)^2, \\ q_i &= (\sin\theta_2 \cos 2\theta)^2, \end{aligned} \tag{4}$$

for $i = 1, 2$, while θ_1 and θ_3 are fixed at 0 and $\pi/4$, respectively. Remarkably, for these values of the initial state preparation probabilities η, the optimal probabilities for FRIO discrimination correspond to the interval I for any inner product s between the states $|\phi_i\rangle$.

On the other hand, for $\eta_1 < \eta_2$ we have that the optimal probabilities are given by

$$\begin{aligned} p_1, r_2 &= (\cos 2\theta(\sin\theta_3 \cos\theta_2 \cos\theta_1 - \cos\theta_3 \sin\theta_1) \pm \sin 2\theta(\sin\theta_3 \cos\theta_2 \sin\theta_1 + \cos\theta_3 \cos\theta_1))^2, \\ p_2, r_1 &= (\cos 2\theta(\cos\theta_3 \cos\theta_2 \cos\theta_1 + \sin\theta_3 \sin\theta_1) \pm \sin 2\theta(\sin\theta_3 \cos\theta_1 - \cos\theta_3 \cos\theta_2 \sin\theta_1))^2, \\ q_{1,2} &= \sin\theta_2(\cos 2\theta \cos\theta_1 \pm \sin 2\theta \sin\theta_1)^2, \end{aligned} \tag{5}$$

where the sign $\pm$ is taken according to the state labeled by $i = 1, 2$ to be discriminated in the FRIO process. Hence, the action of U reveals the three possible results associated with the output states which we labeled as $\{|V\rangle|1\rangle, |H\rangle|1\rangle, |V\rangle|2\rangle\}$. Thus, detection at the corresponding output modes is the final step for implementing any POVM described by the operation given in Eq. (3). For FRIO discrimination, the unitary transformation in Eq. (3) allows us to cover all cases belonging to intervals I and II discussed in the last section. Indeed, detection in the $|V\rangle|2\rangle$ mode corresponds to the inconclusive result for both states $|\phi_i\rangle$ (see Fig. 1). On the other hand, detection in the $|V\rangle|1\rangle$ mode corresponds to the success (error) in the discrimination of $|\phi_{1(2)}\rangle$, while a detection in $|H\rangle|1\rangle$ corresponds to the error (success) in the discrimination of $|\phi_{1(2)}\rangle$.

For the case of interval III, the optimal measurement corresponds to a two-outcome projection[61]. In this case, the unitary transformation can be written as follows

$$\begin{aligned} U|\phi_1\rangle|1\rangle &= \sqrt{q_1}|V\rangle|1\rangle + \sqrt{r_1}|H\rangle|1\rangle, \\ U|\phi_2\rangle|1\rangle &= \sqrt{q_2}|V\rangle|1\rangle + \sqrt{p_2}|H\rangle|1\rangle, \end{aligned} \tag{6}$$

where there is no detection at $|V\rangle|2\rangle$ mode. Thus, the detection in $|V\rangle|1\rangle$ corresponds now with the inconclusive result. Then, for $\eta_1 < \eta_2$ in interval III we obtain the following optimal probabilities:

$$\begin{aligned} p_2, r_1 &= (\cos 2\theta \cos\theta_3 \pm \sin 2\theta \sin\theta_3)^2, \\ q_1, q_2 &= (\cos 2\theta \sin\theta_3 \pm \sin 2\theta \cos\theta_3)^2. \end{aligned} \tag{7}$$

To detect the output photons, PerkinElmer single-photon avalanche detectors (APDs) were placed in the trigger path and the outputs of the Sagnac interferometer to record the photon statistics. A coincidence count module receives the signal from the detectors, where the timing delay was adjusted between each detector's output and the heralding trigger signal. We actively control the pump laser power (1 mW), setting a 500 ps coincidence gate to minimize the accidental counts, generating a coincidence rate of $\sim$ 1400 photons pairs per second. This corresponds to a spectral brightness up to $\sim$ 400000 photon pairs (s mW nm)$^{-1}$.

From the above discussion, it is clear that our experimental setup allows us to implement the optimal FRIO POVM for any pair of non-orthogonal states, arbitrary a priori probabilities, and any value of the fixed rate of inconclusive outcomes. This is done by adjusting the values of the angles θ_1, θ_2, and θ_3 on the corresponding wave plates.

Results and discussion

To show the practicality of the FRIO discrimination scheme using our experimental setup, we implemented the discrimination procedure between the two non-orthogonal polarization qubits given in Eq. (2) for a range of state overlaps s. A key feature of our experiment is that we use a single optical device to implement the complete range of FRIO from MED to UD and include any intermediate case. Indeed, the implementation of every strategy depends on the Sagnac interferometer configuration relying on the angles of the half-wave plates $\mathrm{HWP}_1(\theta_1)$, $\mathrm{HWP}_2(\theta_2)$ and $\mathrm{HWP}_3(\theta_3)$, as was shown in Eqs. (4), (5), and (7). To show the utility of the setup, we consider two cases regarding different states preparation probabilities, in which Alice can prepare the states among the cases $\eta_1 = \eta_2 = 0.5$ and $\eta_1 = 0.3$, $\eta_2 = 0.7$ to experimentally validate Bob's discrimination device. Since in the FRIO scheme these probabilities also bias the discriminated (detected) states [see Eq. (1)], Alice sets these probabilities experimentally by changing the integration time of the coincidence detection rate in terms of the settled values of η by the source. Moreover, as we mentioned before, we considered three different rates of inconclusive outcomes, namely $Q \in \{0, Q_0/2, Q_{max}\}$, where the specific values depend on the inner product s and parameters η_i. We recall that these three values of Q correspond to MED ($Q = 0$), UD ($Q = Q_{max}$), and an intermediate case ($Q = Q_0/2$) in FRIO state discrimination.

In a preliminary step, with waveplates $HWP_i(\theta_i)$ set to $\theta_i = 0$, we evaluated the polarization interference visibility ϵ at the output of the interferometer by measuring in both Pauli bases σ_z and σ_x, corresponding to the logical and diagonal polarization bases, respectively. We obtain the mean visibility $\epsilon = 0.981 \pm 0.006$, which is

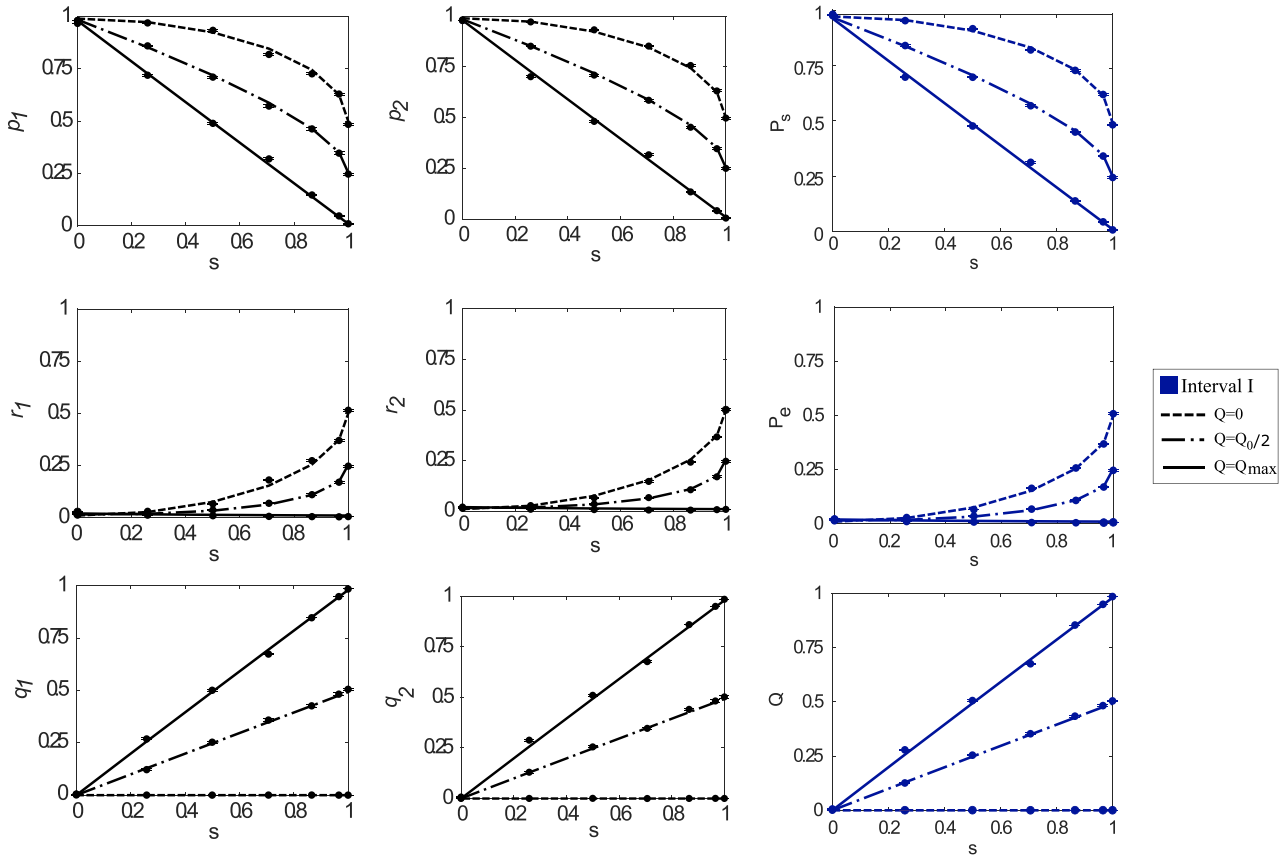

Figure 2. The success P_s, error P_e and inconclusive Q average probabilities as a function of the inner product s, when $\eta_1 = \eta_2 = 0.5$ for both states $|\phi_i\rangle$ are plotted in the third column. The first (second) column shows the success $p_{1(2)}$, error $r_{1(2)}$ and inconclusive $q_{1(2)}$ rates when Alice prepares the state $|\phi_1\rangle$ ($|\phi_2\rangle$) and Bob performs FRIO. The solid and dashed lines in each subplot represent the different values for the mentioned probabilities considering three different values for Q. They were computed using Eq. (8). As was aforementioned, for equally prepared states, we have only access to interval I, which is represented by the blue color in all subplots. Thus, since $\eta_1 = \eta_2$, each state's success, error, and inconclusive rates behavior is the same while the inner product s varies.

typical in polarization-based experiments, where imperfections arise from experimental errors due to laser pump fluctuations in the SPDC process, imperfect spatial mode overlap, and misalignment in the waveplate settings. To take these into account in our comparison between experiment and theory, a white noise model is assumed, considering then the following state received by Bob

$$\rho_i = \epsilon|\phi_i\rangle\langle\phi_i| + \frac{(1-\epsilon)}{2}\mathbb{1}, \tag{8}$$

where $i \in \{1, 2\}$, $\mathbb{1}$ is the identity matrix.

FRIO quantum state discrimination was implemented for state overlap s ranging from orthogonal ($s = 0$) to perfect overlap ($s = 1$). As shown in Eq. (2), the inner product s is set experimentally through the angle of HWP(θ), since $s = \cos 4\theta$. For instance, for $s = 0$ we set $\theta = \pi/8$ to generate $|\phi_1\rangle$, and $\theta = -\pi/8$ to generate $|\phi_2\rangle$. For $s = 1$ we set $\theta = 0$ for both $|\phi_1\rangle$ and $|\phi_2\rangle$. The experimental results are shown in Fig. 2 (for the $\eta_1 = \eta_2 = 0.5$ case), and Fig. 3 (for the $\eta_1 = 0.3, \eta_2 = 0.7$ case). Alice used a data integration time of 10 s for both non-orthogonal states in Fig. 2, while for data in Fig. 3 times of 6 s and 14 s were used for $|\phi_1\rangle$ and $|\phi_2\rangle$, respectively. In both figures we plot the experimental average success P_s, error P_e, and inconclusive probability Q obtained from the recorded success p_i, error r_i, and inconclusive outcome probability q_i related to the state $|\phi_i\rangle$, as shown in Eq. (1). These probabilities are presented as a function of seven different values for the inner product $s \in 0, \ldots, 1$. In Figs. 2 and 3, the first (second) column of plots corresponds to the results obtained when Alice sends the state $|\phi_1\rangle$ ($|\phi_2\rangle$). The right-most column shows the average success, error, and inconclusive probabilities, defined as the sum of these probabilities considering η_1 and η_2 [see Eq. (1)]. Additionally, the expected (theoretical) values of the probabilities are defined in Eq. (1) using slightly mixed states (8) and are depicted by solid lines in every plot.

The error bars are smaller than the experimental points and were obtained with Gaussian error propagation and considering the Poisson statistic of the recorded coincidence counts. We can observe a good agreement between the expected and recorded results for every case regarding different inner product s. Additionally, for the case when $\eta_1 < \eta_2$ showed in Fig. 3, we plot the solid lines with three colors to indicate the three intervals in FRIO. Precisely, the blue color corresponds to interval I, while the green and red colors correspond to intervals II

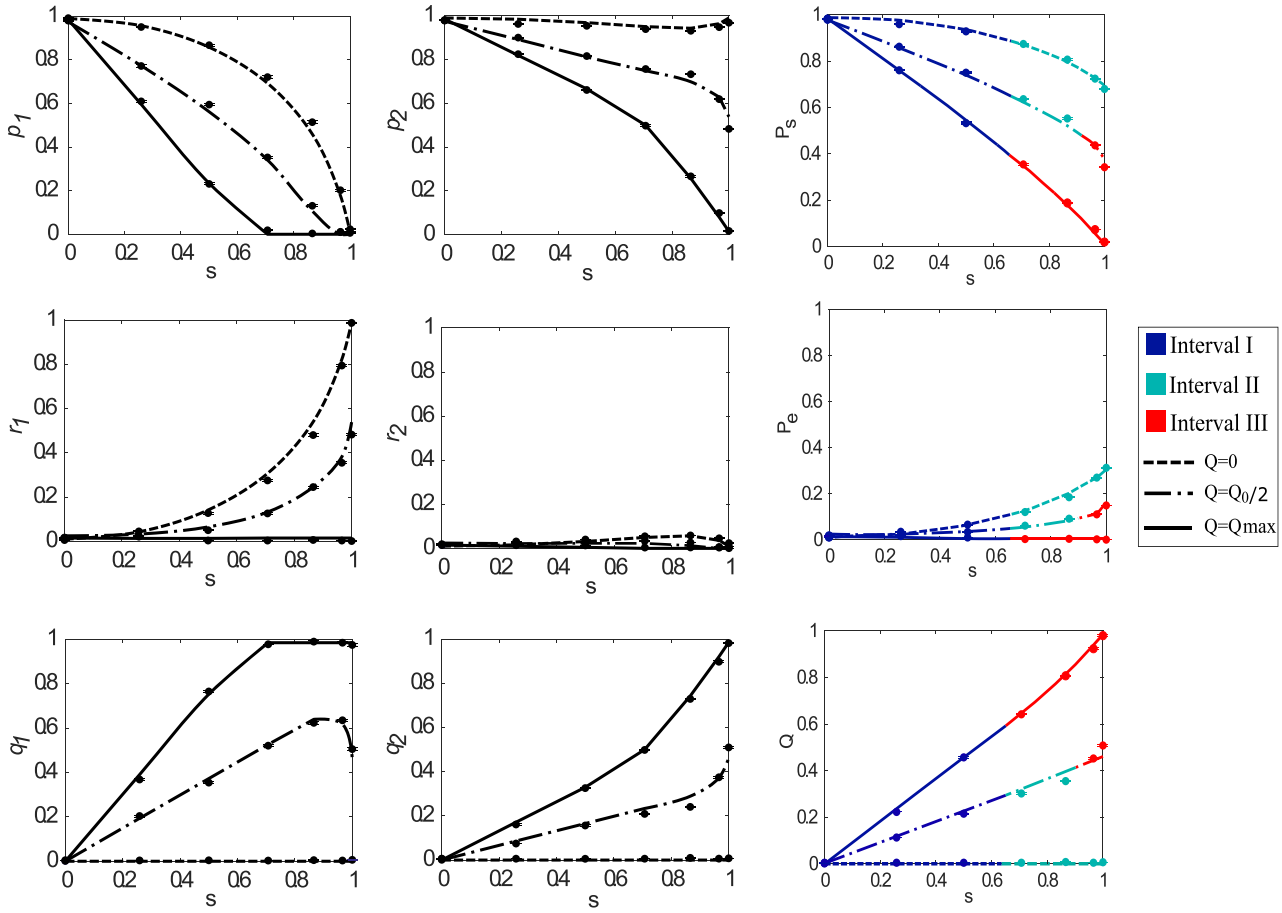

Figure 3. The success P_s (p_i), error P_e (r_i) and inconclusive Q (q_i) probabilities as a function of the inner product s for preparation probabilities given by $\eta_1 = 0.3$ and $\eta_2 = 0.7$. Like Fig. 2, each line in the subplots represents the corresponding probabilities for the state in Eq. (8). Note that the curves in the first and second columns differ due to the preparation probabilities satisfying $\eta_1 \leq \eta_2$. Therefore, the protocol tries to discriminate $|\phi_2\rangle$ better than $|\phi_1\rangle$. However, for optimizing the average success probability P_s, the $|\phi_1\rangle$ must also be considered. Additionally, the three optimization intervals appear for this case, and they are represented by the blue, green, and red colors.

and III, respectively. Although the optimal measurement depends on the interval where the FRIO discrimination is performed, we obtain results close to the expected ones regarding the three intervals. This fact is a signature of the robustness of our platform against different experimental settings, which allow a wide range of discrimination processes contained in the FRIO scheme.

Conclusion. We present a single experimental device capable of discriminating between non-orthogonal polarization states of single photons in the fixed rate of inconclusive outcomes state discrimination scheme, for which the well-known Minimum Error and Unambiguous state discrimination methods are limiting cases. The device is based on a polarization-controlled Sagnac interferometer with nested waveplates and allows for FRIO state discrimination to be implemented for a wide range of parameters, which are defined by the overlap and input statistics of the input states tested. In our setup, Alice controls a photon pair source and encodes non-orthogonal polarization states into a heralded single photon. She sends the photon to Bob, who uses the interferometer to implement a POVM measurement with up to three outcomes. We show that this single device can implement a wide range of state discrimination procedures. Good agreement between theory and experimental results is obtained considering the two-path Sagnac interferometer visibility, which is about 98%. The versatility of the single device makes it directly applicable for quantum information tasks such as quantum communications.

Data Availability

The datasets used and/or analyzed during the current study are available from the corresponding author upon reasonable request.

Received: 12 April 2022; Accepted: 12 October 2022
Published online: 15 October 2022

References

1. Peres, A. *Quantum Theory: Concepts and Methods* (Kluwer Academic, Boston, 1993).
2. Kraus, K. *States, Effects, and Operations: Fundamental Notions of Quantum Theory* (Springer, Berlin, 1983).
3. Tóth, G. & Apellaniz, I. Quantum metrology from a quantum information science perspective. *J. Phys. A Math. Theor.* **47**, 424006. https://doi.org/10.1088/1751-8113/47/42/424006 (2014).
4. Polino, E., Valeri, M., Spagnolo, N. & Sciarrino, F. Photonic quantum metrology. *AVS Quantum Sci.* **2**, 024703. https://doi.org/10.1116/5.0007577 (2020).
5. Nielsen, M. A. & Chuang, I. L. *Quantum Computation and Quantum Information* 10th anniversary edn. (Cambridge University Press, New York, 2010).
6. Bae, J. & Kwek, L.-C. Quantum state discrimination and its applications. *J. Phys. A Math. Theor.* **48**, 083001. https://doi.org/10.1088/1751-8113/48/8/083001 (2015).
7. Bergou, J. A. & Hillery, M. *Introduction to the Theory of Quantum Information Processing. Graduate Texts in Physics* (Springer, New York, 2013).
8. Barnett, S. M. & Croke, S. Quantum state discrimination. *Adv. Opt. Photonics* **1**, 238. https://doi.org/10.1364/AOP.1.000238 (2009).
9. James, D. F. V., Kwiat, P. G., Munro, W. J. & White, A. G. Measurement of qubits. *Phys. Rev. A* **64**, 052312. https://doi.org/10.1103/PhysRevA.64.052312 (2001).
10. Bennett, C. H. Quantum cryptography using any two nonorthogonal states. *Phys. Rev. Lett.* **68**, 3121–3124. https://doi.org/10.1103/PhysRevLett.68.3121 (1992).
11. Roa, L., Delgado, A. & Fuentes-Guridi, I. Optimal conclusive teleportation of quantum states. *Phys. Rev. A* **68**, 022310. https://doi.org/10.1103/PhysRevA.68.022310 (2003).
12. Neves, L., Solís-Prosser, M. A., Delgado, A. & Jiménez, O. Quantum teleportation via maximum-confidence quantum measurements. *Phys. Rev. A* **85**, 062322. https://doi.org/10.1103/PhysRevA.85.062322 (2012).
13. Solís-Prosser, M. A., Delgado, A., Jiménez, O. & Neves, L. Deterministic and probabilistic entanglement swapping of nonmaximally entangled states assisted by optimal quantum state discrimination. *Phys. Rev. A* **89**, 012337. https://doi.org/10.1103/PhysRevA.89.012337 (2014).
14. Delgado, A., Roa, L., Retamal, J. C. & Saavedra, C. Entanglement swapping via quantum state discrimination. *Phys. Rev. A* **71**, 012303. https://doi.org/10.1103/PhysRevA.71.012303 (2005).
15. Chefles, A. Unambiguous discrimination between linearly independent quantum states. *Phys. Lett. A* **239**, 339–347. https://doi.org/10.1016/S0375-9601(98)00064-4 (1998).
16. Marques, B. *et al.* Optimal entanglement concentration for photonic qutrits encoded in path variables. *Phys. Rev. A* **87**, 052327. https://doi.org/10.1103/PhysRevA.87.052327 (2013).
17. Schmid, D. & Spekkens, R. W. Contextual advantage for state discrimination. *Phys. Rev. X* **8**, 011015. https://doi.org/10.1103/PhysRevX.8.011015 (2018).
18. Bera, M. N., Qureshi, T., Siddiqui, M. A. & Pati, A. K. Duality of quantum coherence and path distinguishability. *Phys. Rev. A* **92**, 012118. https://doi.org/10.1103/PhysRevA.92.012118 (2015).
19. Bagan, E., Bergou, J. A. & Hillery, M. Wave-particle-duality relations based on entropic bounds for which-way information. *Phys. Rev. A* **102**, 022224. https://doi.org/10.1103/PhysRevA.102.022224 (2020).
20. Neves, L. *et al.* Control of quantum interference in the quantum eraser. *New J. Phys.* **11**, 073035. https://doi.org/10.1088/1367-2630/11/7/073035 (2009).
21. Jiménez, O., Solís-Prosser, M. A., Neves, L. & Delgado, A. Quantum discord, thermal discord, and entropy generation in the minimum error discrimination strategy. *Entropy*https://doi.org/10.3390/e21030263 *(2019).*
22. Khalid, U., ur Rehman, J. & Shin, H. Measurement-based quantum correlations for quantum information processing. *Sci. Rep.* **10**, 2443. https://doi.org/10.1038/s41598-020-59220-y (2020).
23. Jiménez, O., Solís-Prosser, M., Neves, L. & Delgado, A. Mutual information and quantum discord in quantum state discrimination with a fixed rate of inconclusive outcomes. *Entropy* **23**, 73. https://doi.org/10.3390/e23010073 (2021).
24. Holevo, A. Statistical decision theory for quantum systems. *J. Multivar. Anal.* **3**, 337–394. https://doi.org/10.1016/0047-259X(73)90028-6 (1973).
25. Helstrom, C. W. *Quantum Detection and Estimation Theory* (Academic Press, New York, 1976) OCLC: 316552953.
26. Ivanovic, I. How to differentiate between non-orthogonal states. *Phys. Lett. A* **123**, 257–259. https://doi.org/10.1016/0375-9601(87)90222-2 (1987).
27. Dieks, D. Overlap and distinguishability of quantum states. *Phys. Lett. A* **126**, 303–306. https://doi.org/10.1016/0375-9601(88)90840-7 (1988).
28. Peres, A. How to differentiate between non-orthogonal states. *Phys. Lett. A* **128**, 19. https://doi.org/10.1016/0375-9601(88)91034-1 (1988).
29. Jiménez, O., Sánchez-Lozano, X., Burgos-Inostroza, E., Delgado, A. & Saavedra, C. Experimental scheme for unambiguous discrimination of linearly independent symmetric states. *Phys. Rev. A* **76**, 062107. https://doi.org/10.1103/PhysRevA.76.062107 (2007).
30. Croke, S., Andersson, E., Barnett, S. M., Gilson, C. R. & Jeffers, J. Maximum confidence quantum measurements. *Phys. Rev. Lett.* **96**, 070401. https://doi.org/10.1103/PhysRevLett.96.070401 (2006).
31. Jiménez, O., Solís-Prosser, M. A., Delgado, A. & Neves, L. Maximum-confidence discrimination among symmetric qudit states. *Phys. Rev. A* **84**, 062315. https://doi.org/10.1103/PhysRevA.84.062315 (2011).
32. Herzog, U. Optimized maximum-confidence discrimination of N mixed quantum states and application to symmetric states. *Phys. Rev. A* **85**, 032312. https://doi.org/10.1103/PhysRevA.85.032312 (2012).
33. Chefles, A. Quantum state discrimination. *Contemp. Phys.* **41**, 401–424. https://doi.org/10.1080/00107510010002599 (2000).
34. Chefles, A. & Barnett, S. M. Optimum unambiguous discrimination between linearly independent symmetric states. *Phys. Lett. A* **250**, 223–229. https://doi.org/10.1016/S0375-9601(98)00827-5 (1998).
35. He, B. & Bergou, J. A. A general approach to physical realization of unambiguous quantum-state discrimination. *Phys. Lett. A* **356**, 306–311. https://doi.org/10.1016/j.physleta.2006.03.076 (2006).
36. Reck, M., Zeilinger, A., Bernstein, H. J. & Bertani, P. Experimental realization of any discrete unitary operator. *Phys. Rev. Lett.* **73**, 58–61. https://doi.org/10.1103/PhysRevLett.73.58 (1994).
37. Bergou, J. A., Hillery, M. & Sun, Y. Non-unitary transformations in quantum mechanics: An optical realization. *J. Mod. Opt.* **47**, 487–497. https://doi.org/10.1080/09500340008244054 (2000).
38. Han, R., Leuchs, G. & Bergou, J. A. Helstrom measurement: A nondestructive implementation. *Phys. Rev. A* **101**, 032103. https://doi.org/10.1103/PhysRevA.101.032103 (2020).
39. Clarke, R. B. M. *et al.* Experimental realization of optimal detection strategies for overcomplete states. *Phys. Rev. A* **64**, 012303. https://doi.org/10.1103/PhysRevA.64.012303 (2001).
40. Barnett, S. M. & Riis, E. Experimental demonstration of polarization discrimination at the Helstrom bound. *J. Mod. Opt.* **44**, 1061–1064. https://doi.org/10.1080/09500349708230718 (1997).
41. Higgins, B. L. *et al.* Mixed state discrimination using optimal control. *Phys. Rev. Lett.* **103**, 220503. https://doi.org/10.1103/PhysRevLett.103.220503 (2009).

42. Lu, Y. *et al.* Minimum-error discrimination of entangled quantum states. *Phys. Rev. A* **82**, 042340. https://doi.org/10.1103/PhysRevA.82.042340 (2010).
43. Waldherr, G. *et al.* Distinguishing between nonorthogonal quantum states of a single nuclear spin. *Phys. Rev. Lett.* **109**, 180501. https://doi.org/10.1103/PhysRevLett.109.180501 (2012).
44. Solís-Prosser, M., Fernandes, M., Jiménez, O., Delgado, A. & Neves, L. Experimental minimum-error quantum-state discrimination in high dimensions. *Phys. Rev. Lett.* **118**, 100501. https://doi.org/10.1103/PhysRevLett.118.100501 (2017).
45. Clarke, R. B. M., Chefles, A., Barnett, S. M. & Riis, E. Experimental demonstration of optimal unambiguous state discrimination. *Phys. Rev. A* **63**, 040305. https://doi.org/10.1103/PhysRevA.63.040305 (2001).
46. Mohseni, M., Steinberg, A. M. & Bergou, J. A. Optical realization of optimal unambiguous discrimination for pure and mixed quantum states. *Phys. Rev. Lett.* **93**, 200403. https://doi.org/10.1103/PhysRevLett.93.200403 (2004).
47. Solís-Prosser, M. A., Jiménez, O., Delgado, A. & Neves, L. Enhanced discrimination of high-dimensional quantum states by concatenated optimal measurement strategies. *Quantum Sci. Technol.* **7**, 015017. https://doi.org/10.1088/2058-9565/ac37c4 (2021).
48. Solís-Prosser, M. A. *et al.* Experimental multiparty sequential state discrimination. *Phys. Rev. A* **94**, 042309. https://doi.org/10.1103/PhysRevA.94.042309 (2016).
49. Mosley, P. J., Croke, S., Walmsley, I. A. & Barnett, S. M. Experimental realization of maximum confidence quantum state discrimination for the extraction of quantum information. *Phys. Rev. Lett.* **97**, 193601. https://doi.org/10.1103/PhysRevLett.97.193601 (2006).
50. Steudle, G. A. *et al.* Experimental optimal maximum-confidence discrimination and optimal unambiguous discrimination of two mixed single-photon states. *Phys. Rev. A* **83**, 050304. https://doi.org/10.1103/PhysRevA.83.050304 (2011).
51. Fields, D., Han, R., Hillery, M. & Bergou, J. A. Extracting unambiguous information from a single qubit by sequential observers. *Phys. Rev. A* **101**, 012118. https://doi.org/10.1103/PhysRevA.101.012118 (2020).
52. Mizuno, J. *et al.* Optimum detection for extracting maximum information from symmetric qubit sets. *Phys. Rev. A* **65**, 012315. https://doi.org/10.1103/PhysRevA.65.012315 (2001).
53. Dušek, M. & Bužek, V. Quantum-controlled measurement device for quantum-state discrimination. *Phys. Rev. A* **66**, 022112. https://doi.org/10.1103/PhysRevA.66.022112 (2002).
54. Bergou, J. A. & Hillery, M. Universal programmable quantum state discriminator that is optimal for unambiguously distinguishing between unknown states. *Phys. Rev. Lett.* **94**, 160501. https://doi.org/10.1103/PhysRevLett.94.160501 (2005).
55. Hayashi, A., Hashimoto, T. & Horibe, M. Reexamination of optimal quantum state estimation of pure states. *Phys. Rev. A* **72**, 032325. https://doi.org/10.1103/PhysRevA.72.032325 (2005).
56. Bergou, J. A., Bužek, V., Feldman, E., Herzog, U. & Hillery, M. Programmable quantum-state discriminators with simple programs. *Phys. Rev. A* **73**, 062334. https://doi.org/10.1103/PhysRevA.73.062334 (2006).
57. Probst-Schendzielorz, S. T. *et al.* Unambiguous discriminator for unknown quantum states: An implementation. *Phys. Rev. A* **75**, 052116. https://doi.org/10.1103/PhysRevA.75.052116 (2007).
58. Zhou, T. Unambiguous discrimination between two unknown qudit states. *Quantum Inf. Process.* **11**, 1669–1684. https://doi.org/10.1007/s11128-011-0327-x (2012).
59. Chen, H., Wossnig, L., Severini, S., Neven, H. & Mohseni, M. Universal discriminative quantum neural networks. *Quantum Mach. Intell.* **3**, 1. https://doi.org/10.1007/s42484-020-00025-7 (2021).
60. Patterson, A. *et al.* Quantum state discrimination using noisy quantum neural networks. *Phys. Rev. Res.* **3**, 013063. https://doi.org/10.1103/PhysRevResearch.3.013063 (2021).
61. Bagan, E., Muñoz-Tapia, R., Olivares-Rentería, G. A. & Bergou, J. A. Optimal discrimination of quantum states with a fixed rate of inconclusive outcomes. *Phys. Rev. A* **86**, 040303. https://doi.org/10.1103/PhysRevA.86.040303 (2012).
62. Zhang, C.-W., Li, C.-F. & Guo, G.-C. General strategies for discrimination of quantum states. *Phys. Lett. A* **261**, 25–29. https://doi.org/10.1016/S0375-9601(99)00566-6 (1999).
63. Eldar, Y. C. Mixed-quantum-state detection with inconclusive results. *Phys. Rev. A* **67**, 042309. https://doi.org/10.1103/PhysRevA.67.042309 (2003).
64. Fiurášek, J. & Ježek, M. Optimal discrimination of mixed quantum states involving inconclusive results. *Phys. Rev. A* **67**, 012321. https://doi.org/10.1103/PhysRevA.67.012321 (2003).
65. Herzog, U. Optimal measurements for the discrimination of quantum states with a fixed rate of inconclusive results. *Phys. Rev. A* **91**, 042338. https://doi.org/10.1103/PhysRevA.91.042338 (2015).
66. Herzog, U. Optimal state discrimination with a fixed rate of inconclusive results: Analytical solutions and relation to state discrimination with a fixed error rate. *Phys. Rev. A* **86**, 032314. https://doi.org/10.1103/PhysRevA.86.032314 (2012).
67. Jiménez, O., Solís-Prosser, M. A., Neves, L. & Delgado, A. Mutual information and quantum discord in quantum state discrimination with a fixed rate of inconclusive outcomes. *Entropy* **23**, 73. https://doi.org/10.3390/e23010073 (2021).
68. Zhang, W.-H. & Ren, G. State discrimination of two pure states with a fixed rate of inconclusive answer. *J. Mod. Opt.* **65**, 192–199. https://doi.org/10.1080/09500340.2017.1382592 (2018).
69. Shehu, A. Quantum State Discrimination and Quantum Cloning: Optimization and Implementation. Ph.D. thesis, City University of New York (2015).
70. Ljunggren, D. & Tengner, M. Optimal focusing for maximal collection of entangled narrow-band photon pairs into single-mode fibers. *Phys. Rev. A* **72**, 062301. https://doi.org/10.1103/PhysRevA.72.062301 (2005).
71. Almeida, M. P. *et al.* Environment-induced sudden death of entanglement. *Science* **316**, 579. https://doi.org/10.1126/science.1139892 (2007).
72. Gómez, S. *et al.* Experimental nonlocality-based randomness generation with nonprojective measurements. *Phys. Rev. A* **97**, 040102. https://doi.org/10.1103/PhysRevA.97.040102 (2018).
73. Gómez, E. S. *et al.* Device-independent certification of a nonprojective qubit measurement. *Phys. Rev. Lett.* **117**, 260401. https://doi.org/10.1103/PhysRevLett.117.260401 (2016).

Acknowledgements

This work was supported by the Fondo Nacional de Desarrollo Científico y Tecnológico (FONDECYT) (Grant Nos. 3210359, 1180558, 1190901, 1200266, and 1200859), internal grant from Universidad Mayor (PEP I-2019020), and the National Agency of Research and Development (ANID) – Millennium Science Initiative Program – ICN17–012.

Author contributions

S.G., E.S.G., S.P.W., and G.L. designed and performed the experiment. O.J. and A.D. developed the method presented in the manuscript. All authors wrote and revised the manuscript, gave their opinion, and rewrote different sections of the manuscript.

Competing interests
The authors declare no competing interests.

Additional information
Supplementary Information The online version contains supplementary material available at https://doi.org/10.1038/s41598-022-22314-w.

Correspondence and requests for materials should be addressed to E.S.G.

Reprints and permissions information is available at www.nature.com/reprints.

Publisher's note Springer Nature remains neutral with regard to jurisdictional claims in published maps and institutional affiliations.